

Robust Radar SLAM for Vehicle Parking Applications

Luis Diener, Jens Kalkkuhl, Markus Enzweiler

Abstract—We address ego-motion estimation for automated parking, where centimeter-level accuracy is crucial due to tight spaces and nearby obstacles. Traditional methods using inertial-measurement units and wheel encoders require calibration, making them costly and time-consuming. To overcome this, we propose a radar-based simultaneous localization and mapping (SLAM) approach that leverages the robustness of radar to adverse weather and support for online calibration. Our robocentric formulation fuses feature positions and Doppler velocities for robust data association and filter convergence. Key contributions include a Doppler-augmented radar SLAM method, multi-radar support and an information-based feature-pruning strategy. Experiments demonstrate high-accuracy localization and improved robustness over state-of-the-art methods, meeting the demands of automated parking.

I. INTRODUCTION

Accurate ego-motion estimation is critical for automated parking applications, where the vehicle executes low-speed maneuvers in complex environments. Unlike highway or urban driving, parking scenarios demand centimeter-level accuracy due to space constraints and the proximity to surrounding static and dynamic obstacles. The vehicle must follow the planned trajectory precisely, avoiding obstacles while using the available space most effectively. Increasing the accuracy of ego motion thus allows for lower safety margins, enabling the system to navigate into tighter parking spaces.

The ego-motion states describe the vehicle's movement relative to an earth-fixed reference frame, such as its attitude relative to the ground plane, velocity vector, and position. Traditionally, automotive ego-motion estimation has relied heavily on proprioceptive sensors, including inertial measurement units (IMUs), wheel encoders, and steering angle sensors [1]. These sensors are known for their reliability, availability, and high update rates, making them capable of meeting automotive safety requirements. With the entry of automated driving functions into modern vehicles, additional sensors are required to perceive the vehicle's environment, i.e. cameras and radar sensors. As a result, these sensors have become standard in new vehicles.

Since Global Navigation Satellite Systems (GNSS) in automotive applications cannot provide the required accuracy for automated parking, current solutions rely on the fusion of IMU and wheel-odometry information. Additional vehicle

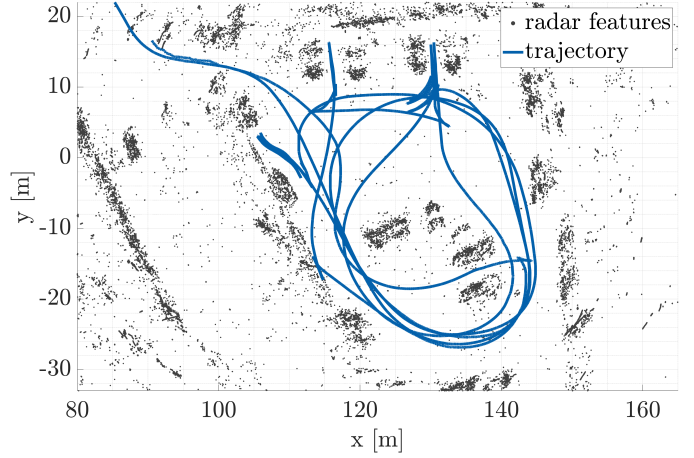


Fig. 1. Our proposed radar SLAM algorithm on a parking space with the vehicle performing several parking maneuvers. Depicted are both the trajectory of the ego vehicle and the tracked features.

model assumptions are necessary to achieve the required performance. Moreover, both IMU and wheel odometry require online calibration; and the vehicle-model assumptions are dependent on external factors such as the vehicle type, the tires or the weight distribution. Thus, significant effort is put into calibrating whole vehicle lines and vehicle types, which is both time-consuming and costly.

Radar-based Simultaneous Localization and Mapping (SLAM) presents a promising solution to these challenges. Radar sensors are inherently robust to adverse weather, low-light conditions, and environments with limited visual features [2]. Furthermore, radar sensors can be calibrated online, which reduces the vehicle-calibration effort. SLAM introduces stationary objects into the motion estimation, which increases the localization accuracy. This is especially relevant during parking maneuvers, where the same features can be observed over an extended period of time.

In this paper, we propose to use a robocentric formulation of the radar SLAM problem. Data association is performed using the 4-dimensional measurement information from the radar sensor, i.e. object position and Doppler velocity. Furthermore, we tightly couple the Doppler-velocity update with the SLAM features.

The main contributions are:

- A novel radar-based SLAM algorithm using both Doppler and position information in the update step with a robocentric feature description for robust data association and filter convergence.

This work has been submitted to the IEEE for possible publication. Copyright may be transferred without notice, after which this version may no longer be accessible.

L. Diener and J. Kalkkuhl are with Mercedes-Benz AG, Germany.

M. Enzweiler is with the Institute for Intelligent Systems, Esslingen University of Applied Sciences, Germany.

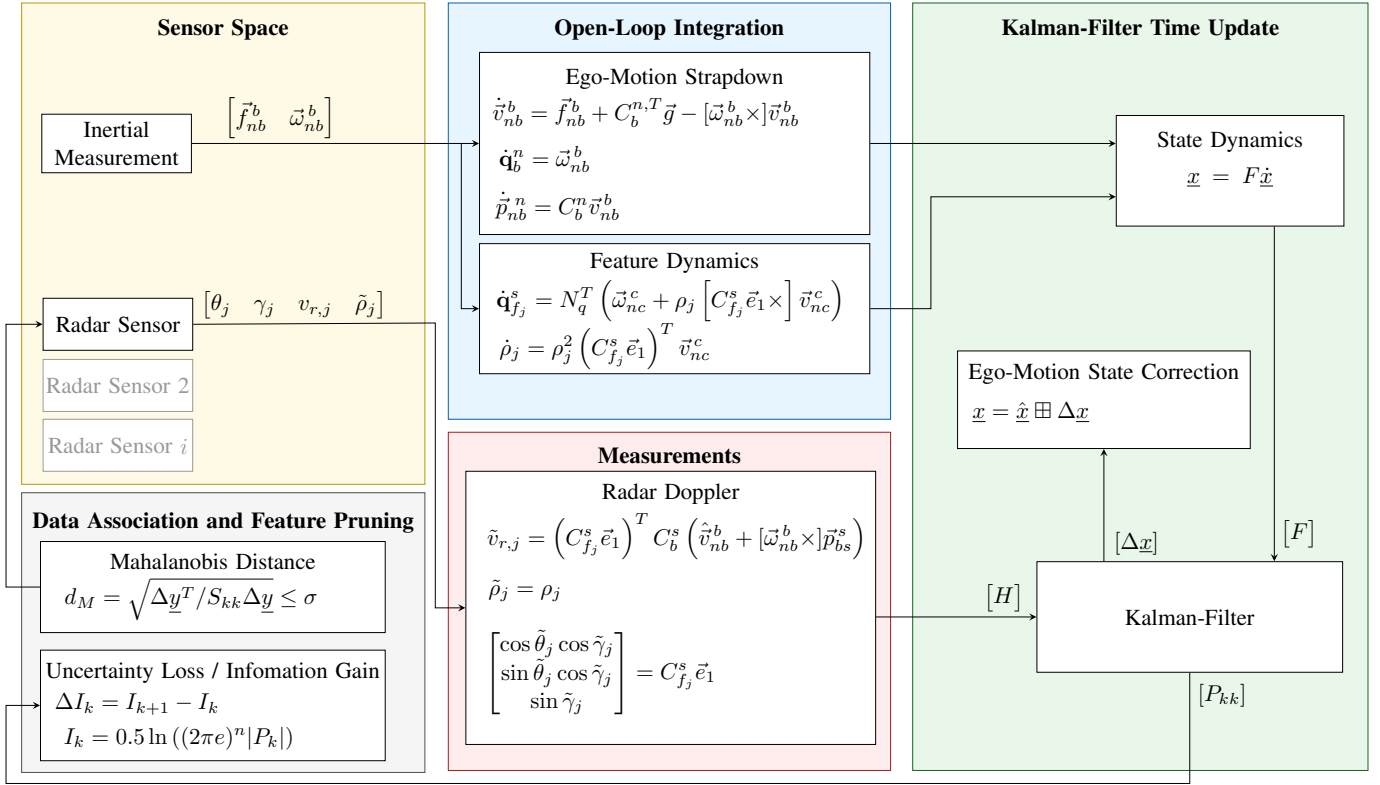


Fig. 2. Overview of the proposed method. Depicted are the sensor input space, the open-loop integration of both the ego-motion states and the feature positions, the radar measurement equations, the mahalanobis-distance-based data association and information-based feature pruning as well as the Kalman filter time update.

- An extension to multi-radar systems, where features are tracked and matched using all the available information.
- A feature-pruning strategy based on the provided information content.

II. RELATED WORK

A. Radar Odometry

Kellner et al. [3] introduced a well-known radar-only approach for ego-motion estimation, which computes the vehicle's velocity and yaw rate. Building on this work, Barjenbruch et al. [4] improved the methodology by incorporating the spatial movement of detections, using a gaussian mixture model. The method aligns with the approaches presented in later studies [5], [6], [7], which offer further improvements in handling uncertainties and correspondence matching [8], [9]. Monaco and Brennan [10] contributed by decoupling translational and rotational motions, using Doppler and spatial data respectively utilizing non-linear optimization to estimate rotational motion.

The integration of radar with other sensors has also been explored, such as in the work by Doer and Trommer [11] to fuse radar-Doppler measurements with inertial data. Harbers et al. [12] adopted a similar approach, where they directly integrated radar Doppler measurements into an extended Kalman filter. Diener et al. [13], [14] incorporate online sensor and

parameter estimation to improve the overall accuracy of ego-motion estimation for normal driving.

In summary, the usage of radar-Doppler measurements allows for robust and accurate ego-motion estimation. In combination with spatial information, other sensors and online calibration, researchers refined their methods further improving performance and robustness. The focus of these approaches lies in estimating the velocity of the vehicle, i.e. the longitudinal and lateral velocities as well as the yaw-rate. To achieve the centimeter-level accuracy required for parking applications, these velocity estimates are still too inaccurate and quickly cause a drift of the position estimate.

B. Localization

SLAM places a strong emphasis on localization, whereas the previously discussed radar-odometry approaches focus on velocity. The majority of recent developments in SLAM stem from visual or visual-inertial systems, which dominate the literature in this field. Nevertheless, the design choices and methodological differences within SLAM frameworks are mostly sensor independent.

One major distinction arises from the choice between filter-based and batch optimization methods. While batch optimization methods typically offer higher accuracy, they do so at the expense of increased computational demands. Among the most well-known SLAM systems are ORB-SLAM [15] and OKVIS

[16], which use keyframe-based optimization in monocular and stereo camera setups.

A critical design decision in SLAM concerns the parameterization of features, particularly in filter-based approaches where features are part of the system state. The conventional approach uses global 3D landmarks, that remain static in the world frame. However, to improve filter linearity and overall estimation consistency, several alternative representations have been proposed. For example, Civera et al. [17] separate depth and bearing components instead of representing features as full 3D vectors. Robocentric parameterizations, which model features in a vehicle-centric frame, have been shown to enhance filter consistency, as investigated by Huai et al. [18]. Furthermore, Bloesch et al. [19] introduce a minimal representation based on the unit sphere S^2 , which reduces the dimensionality and improves the robustness of feature tracking.

Although most SLAM research focuses on visual or visual-inertial systems [20], radar-based localization is gaining interest due to its robustness in adverse environmental conditions. For instance, Michalczyk et al. [21] propose a radar-inertial system that uses both radar distance and Doppler-velocity measurements to update the ego-motion state based on stochastic cloning. Other works focus on graph-based optimization [22], where Doppler information is used as a constraint [23] and IMU data provides further refinements [2]. Loop detection and cl is also a main focus to improve long-term accuracy [24], where the integration of Doppler measurements seems to have further positive effects on the overall accuracy as well [25].

Currently, there is a lack of focus on high-accuracy, short-term localization for applications such as automated parking. Existing approaches rarely utilize multiple radar sensors, and cross-matching of features is typically not performed. Furthermore, Doppler measurements are not coupled with estimated feature positions, leaving potential accuracy gains untapped. Our work aims to address these gaps by exploring tightly coupled multi-radar systems for precise, short-term localization and motion estimation.

III. SYSTEM DESCRIPTION

A. Coordinate Systems

We define the following coordinate systems:

1) *Reference-inertial coordinate system (n)*: Simplified coordinate system that rotates with the earth. We neglect this rotation and thus define it as our inertial system. As further simplification, we define the origin of this coordinate system close to the current position of the vehicle. This way, the x and y axes are tangent to the earth's ellipsoid, while the z axis is aligned with the gravitational vector.

2) *Body-fixed coordinate system (b)*: This coordinate system is connected to the body of the vehicle. The x axis points towards the vehicle's front, while the y axis points to the left and the z axis points up. The origin lies at the center of the vehicle's rear axis. The attitude of the body fixed system with respect to the inertial system can be described using an Euler representation with pitch, roll, yaw [1].

3) *Sensor coordinate system (s)*: A coordinate system that is attached to the body-fixed frame. It is aligned with the sensor and has its origin at the sensor's position.

4) *Feature coordinate system (f)*: A coordinate system that is attached to the earth-fixed frame and has its origin at the feature's position. Since we use point features, the coordinate system's orientation is irrelevant.

A vector \vec{v} that describes motion between coordinate system (n) and coordinate system (b) from the view of coordinate system (s) is denoted as \vec{v}_{nb}^s . Measured quantities are depicted as $\tilde{\bullet}$, whenever this distinction is necessary.

Fig. 1 depicts an overview of the proposed method including the most important equations. While we describe the extension to multi-radar systems and also hinted towards it in Fig. 1, all the depictions are for a single radar sensor.

B. Motion Model

The motion model describes the vehicle's body-fixed velocity \vec{v}_{nb}^b , its attitude \mathbf{q}_b^n and the position \vec{p}_{nb}^n using inertial measurements as inputs. The derivatives of these states are expressed as [26]

$$\dot{\vec{v}}_{nb}^b = \tilde{f}_{nb}^b + C(\mathbf{q}_b^n)^T \vec{g} - [\tilde{\omega}_{nb}^b \times] \vec{v}_{nb}^b \quad (1)$$

$$\dot{\mathbf{q}}_b^n = \tilde{\omega}_{nb}^b \quad (2)$$

$$\dot{\vec{p}}_{nb}^n = C(\mathbf{q}_b^n) \vec{v}_{nb}^b \quad (3)$$

with $\vec{g} = [0 \ 0 \ 9.81\text{m/s}^2]^T$, the direction cosine matrix $C(\mathbf{q}_b^n) = C_b^n$, the measured specific force \tilde{f}_{nb}^b , the measured turning rates $\tilde{\omega}_{nb}^b$, where the symbol $\{\bullet\}$ indicates quaternion multiplication and where $[\tilde{\omega}_{nb}^b \times]$ is a skew-symmetric matrix. The dynamic state vector becomes

$$\underline{x}_I = \begin{bmatrix} \vec{v}_{nb}^b \\ \mathbf{q}_b^n \\ \vec{p}_{nb}^n \end{bmatrix} \quad (4)$$

Hertzberg et al. [27] introduced the boxplus \boxplus operator for filter frameworks. This way, state spaces that lie on manifolds integrate into the standard Kalman filter framework with lower effort. For the time update and state propagation, the boxplus operator is used instead of normal addition. For quaternions the operators are defined as follows [19]:

$$\boxplus : SO(3) \times \mathbb{R}^3 \rightarrow SO(3), \quad \mathbf{q}, \psi \mapsto \exp(\psi) \bullet \mathbf{q} \quad (5)$$

We extract the following Jacobians with respect to the dynamic states:

$$\frac{\partial \dot{\vec{v}}_{nb}^b}{\partial \vec{v}_{nb}^b} = -[\tilde{\omega}_{nb}^b \times] \quad (6)$$

$$\frac{\partial \dot{\vec{v}}_{nb}^b}{\partial \mathbf{q}_b^n} = C_b^{n,T} [\vec{g} \times] \quad (7)$$

$$\frac{\partial \dot{\vec{p}}_{nb}^n}{\partial \vec{v}_{nb}^b} = C_b^n, \quad \frac{\partial \dot{\vec{p}}_{nb}^n}{\partial \mathbf{q}_b^n} = -[C_b^n \tilde{\omega}_{nb}^b \times] \quad (8)$$

C. Relative Feature Motion

The stationary features exhibit a relative motion, that is entirely dependent on the vehicle's ego motion. Bloesch et al. [19] propose to parameterize features on the unit sphere S^2 . This, for once, separates depth and bearing, which is especially relevant in vision-based approaches. However, this parameterization is also advantageous for radar sensors, since they measure both range and bearing independently. The bearing $\mathbf{q}_{f_j}^s$ of a feature j is calculated as [19]:

$$\vec{p}_{sf_j}^s = C \left(\mathbf{q}_{f_j}^s \right) \vec{e}_1 \quad (9)$$

The matrix $C_{f_j}^s$ rotates the basis vector e_1 from the feature direction into the radar sensor coordinate system. $e_{1/2/3} \in \mathbb{R}^3$ describe the basis vectors of an orthonormal coordinate system. We also define the projection matrix:

$$N \left(\mathbf{q}_{f_j}^s \right) = C_{f_j}^s \begin{bmatrix} \vec{e}_2 & \vec{e}_3 \end{bmatrix} = N_q \in \mathbb{R}^{3 \times 2} \quad (10)$$

This matrix is orthogonal to the bearing vector $\vec{p}_{sf_j}^s$ and is used to reduce the axis-angle representation to this orthogonal plane [28].

The feature dynamics are given as [19] [28]:

$$\dot{\mathbf{q}}_{f_j}^s = -N_q^T \left(\vec{\omega}_{ns}^s + \rho_j \left[C_{f_j}^s \vec{e}_1 \times \right] \vec{v}_{ns}^s \right) \quad (11)$$

$$\dot{\rho}_j = - \left(C_{f_j}^s \vec{e}_1 \right)^T \vec{v}_{ns}^s \quad (12)$$

where the sensor-fixed velocity and turning rates are calculated using

$$\vec{v}_{ns}^s = C_b^s \left(\vec{v}_{nb}^b + [\vec{\omega}_{nb}^b \times] \vec{p}_{bs}^b \right) \quad (13)$$

$$\vec{\omega}_{ns}^s = C_b^s \vec{\omega}_{nb}^b \quad (14)$$

with the radar extrinsic alignment C_b^s and translation \vec{p}_{bs}^b .

The dynamic feature state vector becomes:

$$\underline{x}_f = \begin{bmatrix} \mathbf{q}_{f_1}^{s,T} & \rho_1 & \mathbf{q}_{f_2}^{s,T} & \rho_2 & \cdots & \mathbf{q}_{f_j}^{s,T} & \rho_j \end{bmatrix}^T \quad (15)$$

Bloesch et al. [29] provide the following boxplus operator to handle calculations on the unit sphere:

$$\boxplus : SO(3) \times \mathbb{R}^2 \rightarrow SO(3), \quad \mathbf{q}, u \mapsto \exp(N_q u) \bullet \mathbf{q} \quad (16)$$

Using the general Jacobians [29]

$$\frac{\partial \vec{p}_{sf_j}^s}{\partial \mathbf{q}_{f_j}^s} = - \left[\vec{p}_{sf_j}^s \times \right] N_q \quad (17)$$

$$\frac{\partial N_q^T \vec{r}}{\partial \mathbf{q}_{f_j}^s} = N_q^T \left[\vec{r} \times \right] N_q, \quad (18)$$

where \vec{r} is some vector, we can derive Jacobians for the feature dynamics. With respect to the feature states we receive for the bearing dynamics:

$$\begin{aligned} \frac{\partial \dot{\mathbf{q}}_{f_j}^s}{\partial \mathbf{q}_{f_j}^s} &= N_q^T \left[\left(\omega_{nb}^b + [\vec{p}_{sf_j}^s \times] \frac{\vec{v}_{nb}^b}{\rho_j} \right) \times \right] N_q \\ &\quad + N_q^T \frac{1}{\rho_j} [\vec{v}_{ns}^s \times] [\vec{p}_{sf_j}^s \times] N_q \end{aligned} \quad (19)$$

$$\frac{\partial \dot{\rho}_j}{\partial \rho_j} = N_q^T [\vec{p}_{sf_j}^s \times] \vec{v}_{ns}^s \frac{1}{\rho_j^2} \quad (20)$$

and with respect to the dynamic states:

$$\frac{\partial \dot{\mathbf{q}}_{f_j}^s}{\partial \vec{v}_{ns}^s} = -N_q^T \frac{1}{\rho_j} [\vec{p}_{sf_j}^s \times] \quad (21)$$

The depth dynamics provide the following Jacobians:

$$\frac{\partial \dot{\rho}_j}{\partial \mathbf{q}_{f_j}^s} = -\vec{v}_{ns}^{s,T} [\vec{p}_{sf_j}^s \times] N_q \quad (22)$$

$$\frac{\partial \dot{\rho}_j}{\partial \vec{v}_{ns}^s} = -\vec{p}_{sf_j}^{s,T} \quad (23)$$

D. Radar Measurements

We now introduce a novel set of measurement equations for radar sensor applications. By adopting the unit sphere feature parameterization, we can tightly couple Doppler measurements with tracked features. At the same time, the separation of depth and bearing allows for a proper consideration of the distinct measurement noise characteristics.

The radar sensor measures the position of an object using azimuth $\tilde{\theta}_j$, elevation $\tilde{\gamma}_j$ and range $\tilde{\rho}_j$ measurements. Additionally, it measures the Doppler velocity $\tilde{v}_{r,j}$ of said object. This velocity denotes the relative, radial velocity between the radar sensor and the detected object. Assuming the detected object is stationary, the relationship between the radar's velocity \vec{v}_{ns}^s and the Doppler velocity $\tilde{v}_{r,j}$ becomes

$$\tilde{y}_r = -\tilde{v}_{r,j} \quad (24)$$

$$y_r = \vec{p}_{sf_j}^{s,T} \vec{v}_{ns}^s \quad (25)$$

where $\vec{p}_{sf_j}^{s,T}$ projects the velocity vector \vec{v}_{ns}^s onto the radial direction of the detected object $\{j\}$ using measurements of the azimuth θ_j and elevation γ_j angle. Similarly, the object's position is at

$$\tilde{y}_p = [\cos \tilde{\gamma}_j \cos \tilde{\theta}_j \quad \cos \tilde{\gamma}_j \sin \tilde{\theta}_j \quad \sin \tilde{\gamma}_j]^T \tilde{\rho}_j \quad (26)$$

$$y_p = \vec{p}_{sf_j}^s \rho_j \quad (27)$$

We define three measurement functions, i.e. Doppler, bearing and depth. For the Doppler velocity we derive the Jacobians:

$$\frac{\partial y_r}{\partial \vec{v}_{ns}^s} = \vec{p}_{sf_j}^{s,T} \quad (28)$$

$$\frac{\partial y_r}{\partial \mathbf{q}_{f_j}^s} = \vec{v}_{ns}^{s,T} [\vec{p}_{sf_j}^s \times] N_q \quad (29)$$

The depth is measured directly, which results in a Jacobian of 1 with respect to the particular feature. Last, the bearing measurement

$$\tilde{y}_b = [\cos \tilde{\gamma}_j \cos \tilde{\theta}_j \quad \cos \tilde{\gamma}_j \sin \tilde{\theta}_j \quad \sin \tilde{\gamma}_j]^T \quad (30)$$

$$y_b = \tilde{p}_{sf_j}^s \quad (31)$$

results in the Jacobian

$$\frac{\partial y_b}{\partial \mathbf{q}_{f_j}^s} = [\tilde{p}_{sf_j}^s \times] N_q \quad (32)$$

E. Data Association and Feature Pruning

Data association describes the process of matching features of a particular measurement scan to the features states of the filter. We maintain a fixed number of features within the feature state. Thus, we remove and add features regularly keeping the filter alive. Using our information-based feature-pruning strategy, we keep information-rich features within the state, while discarding outliers quickly.

The standard approach for data association is nearest-neighbor matching (Mahalanobis distance) [30].

$$d_M = \sqrt{\Delta \underline{y}^T / S_{kk} \Delta \underline{y}}, \quad (33)$$

with the innovation covariance S_{kk} . This can provide great results, if the sensor does not produce too much clutter and has a relatively low measurement uncertainty. Neira and Tardos [31] propose a matching strategy that iterates through an interpretation tree, considering the joint-compatibility of all matches. This way, matching with spurious measurements is minimized. Zhang et al. [32] propose a quicker solution, that maximizes the combined likelihood of the combined matches. We found that given our 4-dimensional measurements, the Mahalanobis distance based matching provides sufficiently accurate results. We thus use bearing, range and Doppler measurements for feature matching. While the measurement uncertainty in both azimuth and elevation might produce multiple feature candidates, the Doppler-measurement accuracy often steers the selection process towards a single detection.

Feature pruning is delicate, since on one hand we want to maintain features for as long as possible to increase performance, on the other hand the performance quickly degrades when the filter tracks an insufficient amount of features. Especially during parking we can expect features to remain within the vehicle's field of view for an extended period of time. Whereas, normal driving causes features to quickly be lost.

Some researchers develop heuristics based on feature age, successful tracking and overall filter health [19]. Schneider et al. [33] use the Fisher Information Matrix and then minimize it's inverse to find information-rich measurements. Zhang et al. [34] propose the concept of entropy for feature selection, quantifying the information I each feature would provide in a state update:

$$\Delta I_k = I_{k+1} - I_k \quad (34)$$

$$I_k = 0.5 \ln((2\pi e)^n ||P_k||_2), \quad (35)$$

where P_k is the uncertainty matrix of the dynamic state vector at step k and n is the size of that state.

We propose to use this framework two-fold; first, for feature pruning; second, for feature selection. For feature pruning we maintain a score for each feature that is increased according to Eq. (34), whenever a feature provided a successful update; and is decreased in a similar fashion whenever uncertainty of the dynamic states increases (filter prediction). Features with the lowest scores are then pruned in a regular interval. New features are chosen and initialized using the information (Eq. 34) they provide for the next update.

Our novel feature pruning mechanism thus maximizes the information flow to the filter during both feature pruning and feature selection.

F. Extension to Multi-Radar Systems

We introduce an extension to our formalism that enables cross-feature matching across sensors, improving the accuracy and robustness of our algorithm. In contrast, state-of-the-art radar SLAM approaches, while potentially adaptable to multi-sensor setups, do not support cross-sensor feature association, limiting their performance. This is particularly relevant for parking maneuvers, where the vehicle executes sharp turns in confined spaces. There, feature association often fails, and our cross-feature matching improves robustness.

The features are still parameterized in the coordinate system of the sensor where they were first detected. Thus, measurements from another sensor must be transformed into the respective sensor coordinate system. We transform from the sensor coordinate system, where the feature was first detected (s_1) to the coordinate system of the current sensor (s_2) using:

$$\tilde{p}_{s_2 f_j}^{s_2} = C_b^{s_2} C_{s_1}^b \tilde{p}_{s_1 f_j}^{s_1} \rho_j + C_b^{s_2} (\tilde{p}_{bs_2}^b - \tilde{p}_{bs_1}^b) \quad (36)$$

This also affects the Doppler-velocity update:

$$v_{r,j} = \frac{\tilde{p}_{s_2 f_j}^{s_2, T}}{|\tilde{p}_{s_2 f_j}^{s_2}|} \tilde{v}_{ns_2} \quad (37)$$

Subsequently, the changed measurement equations impact the Jacobians of the filter update and thus also require adjustments.

IV. EXPERIMENTAL RESULTS

For our approach we only use on-board sensors of a consumer-grade vehicle. Additionally, the vehicle is equipped with an RTK-INS system, that provides 2 cm localization accuracy, which is used as ground-truth reference. The IMU of this reference system is one order of magnitude more accurate than the IMU of the vehicle. In total, we use 4 corner radars and an automotive-grade IMU for our algorithm.

A. Small Parking Dataset

The first dataset offers 9 distinct parking maneuvers, each beginning and ending with the vehicle at a standstill. Two primary types of maneuvers are included: parallel parking and perpendicular parking. Representative examples of both types are shown in Fig. 3 (parallel parking) and Fig. 4 (perpendicular parking).

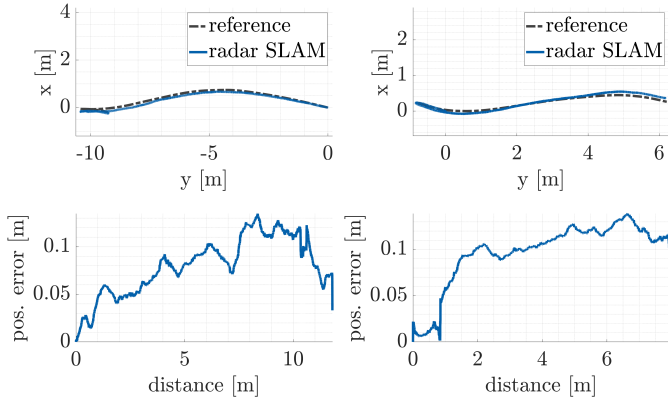


Fig. 3. Localization for two parallel parking maneuvers. The upper plots show the trajectories, while the plots below depict the error between the reference trajectory and the SLAM trajectory.

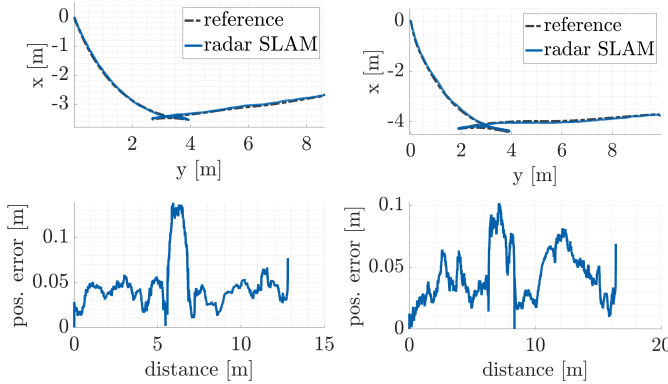


Fig. 4. Localization for two perpendicular parking maneuvers. The upper plots show the trajectories, while the plots below depict the error between the reference trajectory and the SLAM trajectory.

To evaluate the performance of our algorithm, we consider two metrics: the deviation at the end of each maneuver and the root-mean-square error (RMSE) over the entire trajectory. In current parking localization systems, wheel odometry represents the state of the art, consistently achieving end-position accuracy within 20 cm of the true location [35].

Fig. 5 illustrates the relative end-position error of our approach. The radar SLAM algorithm achieves a mean relative end-position error of 9 cm, corresponding to an error of 0.77% w.r.t. the driven distance. The maximum end-position error observed across the dataset is 15 cm. Across all maneuvers the trajectory error averages 8 cm with a maximum of 13 cm.

The proposed radar SLAM algorithm performs well for the parking maneuvers, with a mean deviation below 10 cm. While the results vary, the maximum observed deviation is 15 cm. This accuracy is similar or slightly better than wheel-odometry based approaches. The results indicate that radar-based SLAM is a viable and robust alternative for low-speed, short-range localization tasks.

B. Large Parking Dataset

We use a second dataset consisting exclusively of perpendicular parking maneuvers. Although these maneuvers are simpler in both duration and execution, the increased number

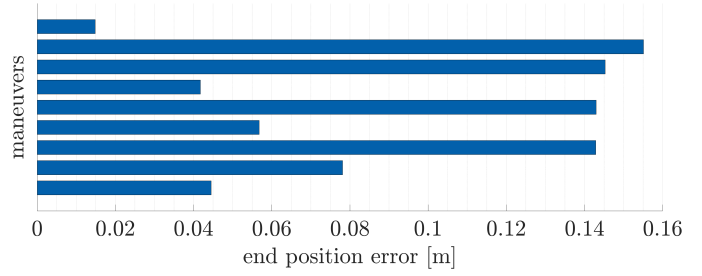


Fig. 5. End-position localization performance for individual parking maneuvers. The end-position error is the final localization error for each individual maneuver.

of samples (45 in total) enables a more robust statistical evaluation.

Table I depicts both the deviation at the maneuver’s end position and the error over the entire trajectory. We evaluate these errors within their 63rd percentile, 95th percentile and maximum values.

In 63% of the test cases (performance threshold) a localization accuracy of 10 cm is achieved with the end position being estimated within 13 cm. Our algorithm achieves a consistent localization performance (95th percentile) of 17 cm with a maximum recorded error of 28 cm.

These results confirm our earlier findings. Our developed algorithm achieves a robust localization accuracy of 20 cm, which coincides with current wheel-odometry-based algorithms [35]. The advantage of the radar-based approach is its robustness against wheel slip and a lower vehicle-calibration effort. Moreover, radar SLAM can be used to calibrate and stabilize wheel-odometry approaches online, further increasing overall accuracy.

TABLE I
EVALUATION OF LOCALIZATION ACCURACY FOR PERPENDICULAR PARKING MANEUVERS.

	63rd percentile	95th percentile	maximum
end pose error	0.13 m	0.24 m	0.28 m
trajectory error	0.10 m	0.17 m	0.28 m

Note: The values for the 63rd and the best 95th percentile indicate that 63% or 95% of all samples have an error of less than or equal to the value provided in the table. Depicted are the both the error at the end of the maneuver and the error over the whole trajectory.

C. Public Datasets

We want to provide a benchmark using publicly available datasets, allowing for better comparison of the approach. We choose the Hercules dataset [36] and the SNAIL radar set [37] as they both offer automotive-grade radar sensors, RTK-INS ground truth and automotive-grade inertial measurements. Moreover, they also include parking scenarios at low speeds. We benchmark against the most recent state-of-the-art radar-based SLAM algorithms, i.e. Radar-ICP (radar-only odometry) [23], RIV-SLAM (radar-inertial SLAM based on graph optimization) [24], RaI-SLAM (Doppler-aided graph optimization) [2] and Doppler-SLAM (Doppler-filter front end with graph-optimization back end) [25]. As evaluation metrics

we use the relative pose error (RPE) as proposed by Wang et al. [24].

Both datasets include low-speed and parking maneuvers, where our approach outperforms state-of-the-art radar SLAM algorithms. Fig. 6 depicts the short-term localization performance for low-speed maneuvers ($v < 10$ m/s) in both datasets. Our algorithm achieves the lowest relative error for these low-speed maneuvers. It benefits at lower speeds, since features then contribute more samples to the filter, increasing accuracy.

While our algorithm remains competitive with state-of-the-art methods during normal driving scenarios ($v \geq 10$ m/s), we observe a performance drop at higher speeds, as shown in Fig. 7. This is primarily due to the rapid loss of features, which limits the information available to the filter and consequently degrades accuracy. Notably, the compared approaches benefit from loop-closure techniques, increasing accuracy in these particular datasets, that start and end at the same location. In real-world driving applications loop closure is much less common. Despite this, we maintain comparable performance.

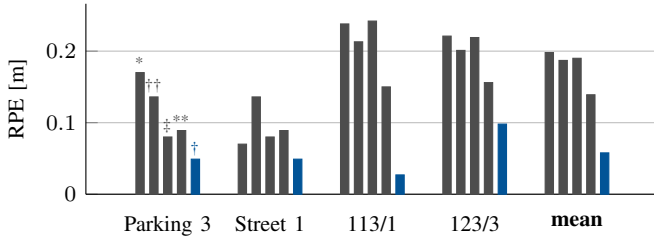


Fig. 6. Public benchmark on parking maneuvers depicting the relative localization error. Displayed are *Radar-ICP [23], ††RIV-SLAM [24], ‡RaI-SLAM [2], **Doppler-SLAM [25], and †our solution.

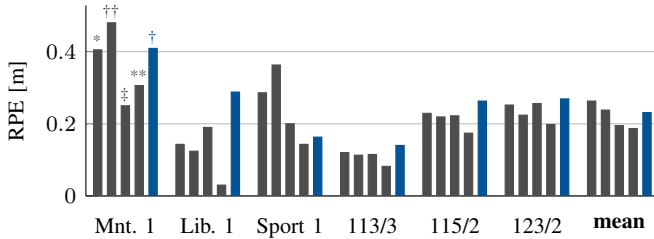


Fig. 7. Public benchmark on driving maneuvers depicting the relative localization error. Displayed are *Radar-ICP [23], ††RIV-SLAM [24], ‡RaI-SLAM [2], **Doppler-SLAM [25], and †our solution.

D. Ablation Study

In our last evaluation, we assess the individual impact of our key contributions on the overall system performance. Specifically, we evaluate the tightly-coupled Doppler-velocity measurement update; cross-sensor feature tracking; and the sensitivity of the system to the number of simultaneously tracked features.

The results are summarized in Tab. II. We observe that reducing the number of tracked features has minimal impact on performance until the number is lowered to 12, at which point the localization accuracy degrades noticeably. Among the evaluated components, the tightly-coupled velocity update yields the largest improvement, with its removal leading to

the largest performance drop overall. Additionally, cross-sensor feature matching shows a clear benefit, confirming that successful tracking across sensors contributes meaningfully to the overall accuracy.

These results demonstrate that our tightly-coupled velocity update and cross-sensor feature tracking are key contributors to the localization accuracy of our algorithm, while our feature pruning strategy even allows for reductions in the number of tracked features.

TABLE II
ABLATION STUDY ON END POSE ERROR OF PERPENDICULAR PARKING MANEUVERS.

	63rd percentile	95th percentile	max.
w/o Doppler velocity	0.20 m	0.37 m	0.58 m
w/o cross matching	<u>0.17 m</u>	0.28 m	0.36 m
1/2 feature count (25)	0.13 m	0.24 m	0.28 m
1/4 feature count (12)	0.16 m	<u>0.29 m</u>	<u>0.48 m</u>
full solution	0.13 m	0.24 m	0.28 m

Note: Values in **bold** indicate the greatest impacts and underlined values indicate the second biggest changes.

V. CONCLUSION

We developed a radar-inertial SLAM algorithm, that performs especially well for parking maneuvers. There, it outperforms state-of-the-art radar SLAM algorithms and achieves performance comparable to state-of-the-art wheel odometry. We showed that this performance is reached consistently using statistical evaluation methods on a large dataset. The robocentric formulation of our SLAM features allows for compact measurement updates, tightly coupling Doppler, bearing and range measurements. Our information-based pruning and matching strategy ensures robust correspondences and consistent filter health. We provided an extension to multi-radar systems which allows for cross-matching of features, which is especially beneficial for parking maneuvers.

Using publicly available datasets, we benchmarked our approach against state-of-the-art radar SLAM approaches and could show increased performance for parking maneuvers.

Future work should focus on the integration and joint calibration of wheel odometry, inertial measurements, and vehicle models. In doing so, wheel-odometry-based approaches can be further refined to achieve the centimeter-level accuracy required for automated parking, while also benefiting from the advantages of radar-based SLAM.

REFERENCES

- [1] V. Rodrigo Marco, J. Kalkkuhl, J. Raisch, W. J. Scholte, H. Nijmeijer, and T. Seel, "Multi-modal sensor fusion for highly accurate vehicle motion state estimation," *CEP*, vol. 100, p. 104409, 2020.
- [2] D. C. Herraiz, M. Zeller, D. Wang, J. Behley, M. Heidingsfeld, and C. Stachniss, "RaI-SLAM: Radar-Inertial SLAM for Autonomous Vehicles," *RA-L*, vol. 10, no. 6, pp. 5257–5264, Jun. 2025.
- [3] D. Kellner, M. Barjenbruch, J. Klappstein, J. Dickmann, and K. Dietmayer, "Instantaneous ego-motion estimation using Doppler radar," in *ITSC 2013*, 2013, pp. 869–874.
- [4] M. Barjenbruch, D. Kellner, J. Klappstein, J. Dickmann, and K. Dietmayer, "Joint spatial- and Doppler-based ego-motion estimation for automotive radars," in *IV 2015*, 2015, pp. 839–844.

- [5] Y. Almalioglu, M. Turan, C. X. Lu, N. Trigoni, and A. Markham, "MilliRIO: Ego-motion estimation with low-cost millimetre-wave radar," *IEEE Sens. J.*, vol. 21, no. 3, pp. 3314–3323, 2021.
- [6] Y. Xu, Q. Huang, S. Shen, and H. Yin, "Incorporating point uncertainty in radar SLAM," *RA-L*, vol. 10, no. 3, pp. 2168–2175, 2025.
- [7] S. Kim, J. Seok, J. Lee, and K. Jo, "Radar4Motion: IMU-Free 4D Radar Odometry with Robust Dynamic Filtering and RCS-Weighted Matching," *T-IV*, pp. 1–11, 2024.
- [8] M. Rapp, M. Barjenbruch, M. Hahn, J. Dickmann, and K. Dietmayer, "Probabilistic ego-motion estimation using multiple automotive radar sensors," *RAS*, vol. 89, pp. 136–146, 2017.
- [9] K. Haggag, S. Lange, T. Pfeifer, and P. Protzel, "A Credible and Robust Approach to Ego-Motion Estimation Using an Automotive Radar," *RA-L*, vol. 7, no. 3, pp. 6020–6027, Jul. 2022.
- [10] C. D. Monaco and S. N. Brennan, "RADARODO: Ego-motion estimation from doppler and spatial data in RADAR images," *T-IV*, vol. 5, no. 3, pp. 475–484, 2020.
- [11] C. Doer and G. F. Trommer, "An EKF based approach to radar inertial odometry," in *MFI 2020*, 2020, pp. 152–159.
- [12] S. Harbers, J. Kalkkuhl, and T. Van Der Sande, "Vehicle Egomotion Estimation Through IMU-RADAR Tight-Coupling," *OJ-ITS*, vol. 6, pp. 244–255, 2025.
- [13] L. Diener, J. Kalkkuhl, and T. Schirle, "Radar-based approach for side-slip gradient estimation," *SAE Technical Paper 2024-01-2976*, Jul. 2024.
- [14] L. Diener, J. Kalkkuhl, and M. Enzweiler, "Radar Misalignment Calibration using Vehicle Dynamics Model," *TechRxiv preprint*, Feb. 2025.
- [15] C. Campos, R. Elvira, J. J. G. Rodríguez, J. M. M. Montiel, and J. D. Tardós, "ORB-SLAM3: An accurate open-source library for visual, visual-inertial, and multimap SLAM," *IEEE T. Robot.*, vol. 37, no. 6, pp. 1874–1890, 2021.
- [16] S. Leutenegger, S. Lynen, M. Bosse, R. Siegwart, and P. Furgale, "Keyframe-based visual-inertial odometry using nonlinear optimization," *IJRR*, vol. 34, no. 3, pp. 314–334, Mar. 2015.
- [17] J. Civera, A. Davison, and J. Montiel, "Inverse Depth Parametrization for Monocular SLAM," *IEEE Trans. Robot.*, vol. 24, no. 5, pp. 932–945, Oct. 2008.
- [18] Z. Huai and G. Huang, "Robocentric visual-inertial odometry," in *IROS 2018*, 2018, pp. 6319–6326.
- [19] M. Bloesch, M. Burri, S. Omari, M. Hutter, and R. Siegwart, "Iterated extended Kalman filter based visual-inertial odometry using direct photometric feedback," *IJRR*, vol. 36, no. 10, pp. 1053–1072, Sep. 2017.
- [20] G. Huang, "Visual-inertial navigation: A concise review," in *ICRA 2019*, 2019, pp. 9572–9582.
- [21] J. Michalczyk, R. Jung, and S. Weiss, "Tightly-Coupled EKF-Based Radar-Inertial Odometry," in *IROS 2022*. Kyoto, Japan: IEEE, Oct. 2022, pp. 12 336–12 343.
- [22] J. Zhang, H. Zhuge, Z. Wu, G. Peng, M. Wen, Y. Liu, and D. Wang, "4DRadarSLAM: A 4D Imaging Radar SLAM System for Large-scale Environments based on Pose Graph Optimization," in *ICRA 2023*. London, United Kingdom: IEEE, May 2023, pp. 8333–8340.
- [23] D. C. Herraiez, M. Zeller, L. Chang, I. Vizzo, M. Heidingsfeld, and C. Stachniss, "Radar-Only Odometry and Mapping for Autonomous Vehicles," in *ICRA 2024*. Yokohama, Japan: IEEE, May 2024, pp. 10 275–10 282.
- [24] D. Wang, S. May, and A. Nuechter, "RIV-SLAM: Radar-Inertial-Velocity optimization based graph SLAM," in *CASE 2024*. Bari, Italy: IEEE, Aug. 2024, pp. 774–781.
- [25] D. Wang, H. Haag, D. C. Herraiez, S. May, C. Stachniss, and A. Nuechter, "Doppler-SLAM: Doppler-Aided Radar-Inertial and LiDAR-Inertial Simultaneous Localization and Mapping," *arXiv:2504.11634 preprint*, Apr. 2025.
- [26] J. Solà, "Quaternion kinematics for the error-state Kalman filter," *preprint*, Nov. 2017.
- [27] R. a. F. Hertzberg, Christoph and Wagner, "Integrating generic sensor fusion algorithms with sound state representations through encapsulation of manifolds," *Infor. Fus.*, vol. 14, no. 1, pp. 57–77, 2013.
- [28] J. Jackson, J. Nielsen, T. McLain, and R. Beard, "Improving the Robustness of Visual-Inertial Extended Kalman Filtering," in *ICRA 2019*. Montreal, QC, Canada: IEEE, May 2019, pp. 4703–4709.
- [29] M. Bloesch, H. Sommer, T. Laidlow, M. Burri, G. Nuetzi, P. Fankhauser, D. Bellicoso, C. Gehring, S. Leutenegger, M. Hutter, and R. Siegwart, "A Primer on the Differential Calculus of 3D Orientations," *arXiv:1606.05285 preprint*, Oct. 2016.
- [30] P. Mahalanobis, "Reprint of: Mahalanobis, P.C. (1936) "On the Generalised Distance in Statistics.," *Sankhya A*, vol. 80, no. 1, pp. 1–7, Dec. 2018.
- [31] J. Neira and J. Tardos, "Data association in stochastic mapping using the joint compatibility test," *RA-L*, vol. 17, no. 6, pp. 890–897, Dec. 2001.
- [32] S. Zhang, L. Xie, and M. Adams, "An Efficient Data Association Approach to Simultaneous Localization and Map Building," *IJRR*, vol. 24, no. 1, pp. 49–60, Jan. 2005.
- [33] T. Schneider, M. Li, C. Cadena, J. Nieto, and R. Siegwart, "Observability-Aware Self-Calibration of Visual and Inertial Sensors for Ego-Motion Estimation," *IEEE Sens. J.*, vol. 19, no. 10, pp. 3846–3860, May 2019.
- [34] Sen Zhang, Lihua Xie, and M. Adams, "Entropy based feature selection scheme for real time simultaneous localization and map building," in *IROS 2005*. Edmonton, Alta., Canada: IEEE, 2005, pp. 1175–1180.
- [35] A. Brunner, T. Wohlgenuth, M. Frey, and F. Gauterin, "Odometry 2.0: A Slip-Adaptive EIF-Based Four-Wheel-Odometry Model for Parking," *T-IV*, vol. 4, no. 1, pp. 114–126, Mar. 2019.
- [36] H. Kim, M. Jung, C. Noh, S. Jung, H. Song, W. Yang, H. Jang, and A. Kim, "HeRCULES: Heterogeneous Radar Dataset in Complex Urban Environment for Multi-session Radar SLAM," *arXiv:2502.01946 preprint*, Feb. 2025.
- [37] J. Huai, B. Wang, Y. Zhuang, Y. Chen, Q. Li, and Y. Han, "SNAIL Radar: A large-scale diverse benchmark for evaluating 4D-radar-based SLAM," *IJRR*, May 2025.